Optics Letters

Extended depth-of-field 3D endoscopy with synthetic aperture integral imaging using an electrically tunable focal-length liquid-crystal lens

YU-JEN WANG,[1] XIN SHEN,[2] YI-HSIN LIN,[1] AND BAHRAM JAVIDI[2,*]

[1]Department of Photonics, National Chiao Tung University, 1001 Ta Hsueh Rd., Hsinchu 30010, Taiwan
[2]Electrical and Computer Engineering Department, University of Connecticut, Storrs, Connecticut 06269-4157, USA
*Corresponding author: bahram.javidi@uconn.edu

Received 23 March 2015; revised 27 June 2015; accepted 29 June 2015; posted 2 July 2015 (Doc. ID 236667); published 27 July 2015

Conventional synthetic-aperture integral imaging uses a lens array to sense the three-dimensional (3D) object or scene that can then be reconstructed digitally or optically. However, integral imaging generally suffers from a fixed and limited range of depth of field (DOF). In this Letter, we experimentally demonstrate a 3D integral-imaging endoscopy with tunable DOF by using a single large-aperture focal-length-tunable liquid crystal (LC) lens. The proposed system can provide high spatial resolution and an extended DOF in synthetic-aperture integral imaging 3D endoscope. In our experiments, the image plane in the integral imaging pickup process can be tuned from 18 to 38 mm continuously using a large-aperture LC lens, and the total DOF is extended from 12 to 51 mm. To the best of our knowledge, this is the first report on synthetic aperture integral imaging 3D endoscopy with a large-aperture LC lens that can provide high spatial resolution 3D imaging with an extend DOF.

OCIS codes: (110.6880) Three-dimensional image acquisition; (110.4190) Multiple imaging; (230.3720) Liquid-crystal devices; (230.2090) Electro-optical devices.

http://dx.doi.org/10.1364/OL.40.003564

Integral photography [1], also known as integral imaging, is one of the main approaches in 3D imaging technologies. It uses a microlens array or a camera array to pick up rays from an object with various perspectives and then reconstructs the original object with an inverse process [2–4]. The captured image, referred to as an elemental image array, conveys the information of direction and intensities of the object.

In general, 3D integral imaging suffers from a fixed and limited range of DOF. Research has been done to improve the resolution and DOF of 3D integral images [5–9]. For biomedical applications, such as microscopy and endoscopy [10,11], high pixel density and short working distance are the essential requirements for the pickup stage. Recently, hexagonal liquid-crystal lenslet arrays for compact 3D integral-imaging endoscopy have been investigated [12]. However, this kind of system still suffers from poor image resolution due to a low numerical aperture of the micro-lenslets. Synthetic-aperture-integral imaging (SAII) replaces the microlens array by a moving camera to record elemental images and provides high resolution during the pickup process [13]. For integral imaging, endoscopes have a short working distance and sensors with small pixel sizes, thus it is a good candidate as the pickup devices. However, the DOF of an endoscope is usually around 30–40 mm. To extend the DOF of an endoscopic imaging system, adding an electrically tunable focusing liquid-crystal (LC) lens as an active optical element has been demonstrated [14]. The orientations of the LC molecules are electrically manipulated to spatially modulate the incident wavefront of light in terms of proper spatial distribution of the refractive indices. The LC lens is capable of functioning as a tunable positive or negative lens [14–16]. Integral imaging systems [2–6] can be aided by LC lens technology to enhance the DOF.

In this Letter, we propose a synthetic-aperture integral imaging for 3D endoscopy with a large aperture LC lens. This approach allows for capturing short depth range objects with not only a high resolution but also an extended DOF. We show by experiments that the image planes in the pickup process can be tuned from 18 to 38 mm using a large-aperture LC lens, and the extended DOF is from 12 to 51 mm. To the best of our knowledge, this is the first report on a 3D synthetic-aperture integral-imaging endoscopy with a large-aperture LC lens for high-resolution 3D imaging with an extended DOF.

The 3D SAII endoscopy image capture process where the camera is mounted on a translation stage is illustrated in Fig. 1(a). The capturing device consists of a polarizer, an LC lens, and an endoscopic imaging system. The endoscopic imaging system is composed of an imaging lens and an image sensor. The imaging lens is a set of solid lenses, also referred to as the lens module. In Fig. 1(a), the position of the whole capturing device is adjustable. The moving steps in the horizontal (H) and vertical (V) axes are set as (P_H, P_V), which depend on the

0146-9592/15/153564-04$15/0$15.00

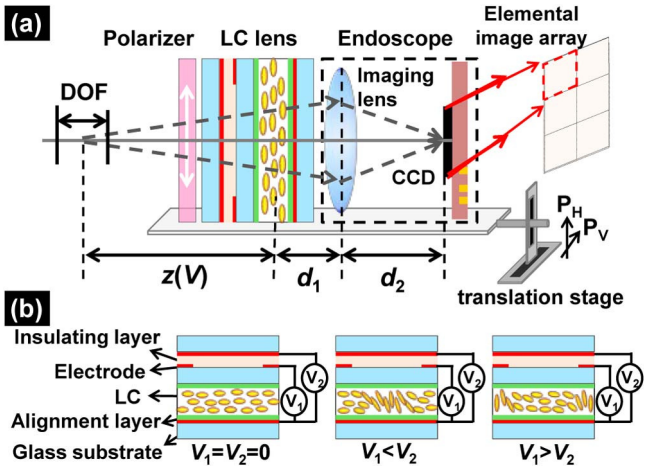

Fig. 1. (a) Illustration of the 3D SAII endoscopy image capture process using an LC lens. The white arrow of the polarizer is the transmissive axis. (b) The operating principle of the LC lens used in (a). When $V_1 = V_2 = 0$, the LC lens has zero lens power. When $V_1 < V_2$, the LC lens is a negative lens with a negative lens power. When $V_1 > V_2$, the LC lens is a positive lens with a positive lens power.

size of the image sensor. By adjusting (P_H, P_V) and capturing the corresponding perspective images of an object at distance z, the elemental images are obtained in the form of an image array. Based on the image formation of a thin lens, the objective distance between the object and the LC lens is [16]

$$z(V_1, V_2) = \frac{1}{D_{\mathrm{LC}}(V_1, V_2) + D_{\mathrm{sys}}}, \tag{1}$$

where V_1 *and* V_2 are the applied voltages to the LC lens, $D_{\mathrm{LC}}(V_1, V_2)$ is the lens power of the LC lens. In Eq. (1), D_{sys} is the effective lens power of the endoscope which is

$$D_{\mathrm{sys}} = -\left[\frac{d_1}{n_g} + \frac{1}{(D_i - 1/d_2)}\right]^{-1}, \tag{2}$$

where d_1 is the distance between the LC lens and the imaging lens and is approximately equal to the thickness of the LC lens, n_g is the refractive index of the glass substrates of the LC lens, D_i is the lens power of the imaging lens, and d_2 is the distance between the imaging lens and the CCD. The DOF is [14]

$$\mathrm{DOF}(V) \propto z(V) = \frac{1}{D_{\mathrm{LC}}(V) + D_{\mathrm{sys}}}. \tag{3}$$

In Eqs. (1) and (3), the elemental images can be recorded with different DOFs by tuning the lens power of the LC lens. This also indicates that the SAII pickup process with a tunable DOF can be realized. As a result, we can reconstruct 3D images of the objects with an extended DOF. By using the depth-estimation method [17], the depth information corresponding to each pixel of the elemental images can be calculated. For practical display, a single elemental image array is needed for a large DOF 3D imaging. Thus, by employing a merged elemental image array extracted from the enhanced DOF images obtained under different applied voltage conditions on the LC lens, the extended DOF integral imaging can be realized.

To demonstrate the proposed system, the LC lens we used is able to be operated as a positive lens or a negative lens, as depicted in Fig. 1(b). The structure of the LC lens is composed by (1) three-layer electrodes coated with indium tin oxide (ITO), (2) three glass substrates with a thickness of 0.7 mm and a refractive index (n_g) of 1.518, (3) insulating layer (NOA81) with a thickness of 25 μm, (4) nematic LC (LCM1790, $\Delta n = 0.43$ for $\lambda = 546$ nm at 21°C) with a thickness of 50 μm, and (5) an alignment layer (polyvinyl alcohol) with a mechanically buffered process for aligning the LC molecules. One of the ITO electrodes was etched with a 2-mm-diameter hole. It provides an inhomogeneous electric field in order to generate proper phase profile resulting from the reorientations of the LC molecules. The applied voltage between the hole-patterned electrode and the bottom electrode is defined as V_1, and the applied voltage between another electrode and the bottom electrode is defined as V_2. At $V_1 = V_2$, the lens power of the LC lens is zero. At $V_1 < V_2$, the LC directors in the center of the aperture are more perpendicular to the glass substrate than the LC directors around the peripheral region. Thus, the LC lens functions as a negative lens. Similarly, at $V_1 > V_2$, the LC directors around the peripheral region are reoriented more perpendicular to the glass substrate than those in center, thus the LC lens functions as a positive lens.

As to measuring the lens power of the LC lens, the LC lens was placed between a pair of crossed polarizers. The rubbing direction of the LC lens was set at 45 deg with respect to the transmissive axis of one polarizer. The light source is a laser diode ($\lambda = 632.8$ nm). The phase profiles of the LC lens operated as a negative lens and positive lens are shown in Figs. 2(a) and 2(b), respectively. The concentric circles in phase profiles indicate the spatial phase retardation between the ordinary wave and the extraordinary wave. Extraordinary and ordinary wave are defined as the electric field polarization of the waves parallel and perpendicular to the director of LC molecule, respectively. From the number of concentric circles, the lens power (D_{LC}) is calculated according to

$$D_{LC} = (8 \cdot N \cdot \lambda)/R^2, \tag{4}$$

where N is the number of the concentric circles, λ is the wavelength, and R is the diameter. In Figs. 2(a) and 2(b), the lens powers are −15.2 m^{-1} and 11.4 m^{-1}, respectively. We also applied different voltages to test the electrically tunable lens power of the LC lens, as shown in Fig. 2(c). In Fig. 2(c), the blue triangles represent the negative lens power of the LC lens at different V_2 while V_1 was fixed as 0 V_{rms}. The tunable range of the negative lens power is from 0 to −15.2 m^{-1}. The red dots represent the positive lens power at different V_2 for fixed V_1 of

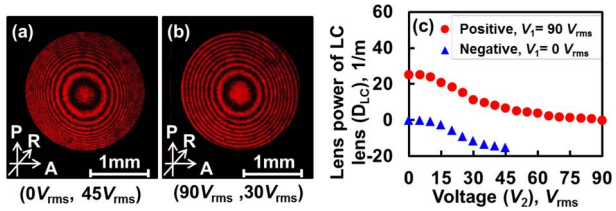

Fig. 2. Phase profiles of the LC lens at (a) (V_1, V_2) = (0, 45 V_{rms}) and (b) (V_1, V_2) = (90 V_{rms}, 30 V_{rms}). P and A stand for the transmissive axes of the polarizer and the analyzer, respectively. R is the rubbing direction of the LC lens. (c) The lens power of the LC lens as a function of the applied voltage V_2.

90 V_{rms}. The positive lens power ranges from 25.32 to 0 m^{-1}. The lens power is continuously tunable at different applied voltages. In the following experiment, the LC lens was set at the lens power of −15.2 m^{-1} as $(V_1, V_2) = (0, 45\ V_{rms})$ and 11.4 m^{-1} as $(V_1, V_2) = (90\ V_{rms}, 30\ V_{rms})$.

To further demonstrate the proposed 3D SAII endoscopy system in Fig. 1(a), the LC lens and a polarizer were attached to an endoscope (Model: nk2794, NewKen Tech. Co. Ltd.). The endoscope consists of (1) an imaging lens with an effective lens power (D_i) of 746.3 m^{-1} (f = 1.34 mm), and (2) a CCD as an image sensor with a resolution of 1280 (H) × 720 (V) pixels, and individual pixel size of 1.4 μm. The distance between the CCD and the imaging lens (d_2) is 1.4 mm. Then a resolution chart (USAF 1951) with a spatial frequency of 3.56 lp/mm was used as our object placed in front of the capturing device. Owing to the fixed d_2 in Fig. 1(a), the object at a certain range of z could be imaged by the image sensor without the LC lens. Using the tunable focusing LC lens, the object at different positive z could be imaged by the image sensor. In the experiment, we adjusted different applied voltages of the LC lens to record the resolution chart at various object distances (z). The corresponding contrast ratio (CR) of a captured image of the resolution chart is defined as $CR = (I_{max} - I_{min})/(I_{max} + I_{min})$, where I_{max} and I_{min} represent the maximum and minimum intensity of each captured image, respectively. Figure 3(a) shows the CR as a function of z when the LC lens was operated as a positive lens, a negative lens, and without lens power. As can be seen from Fig. 3(a), we obtained images with the highest CR when z was at 18 mm for $(V_1, V_2) = (90\ V_{rms}, 30\ V_{rms})$, at 23 mm for $(V_1, V_2) = (0, 0)$, and at 38 mm for $(V_1, V_2) = (0, 45\ V_{rms})$. This also indicates that we can capture focused images when the object is located between z = 18 mm and z = 38 mm by changing the lens power of the LC lens. As for the DOF, we defined DOF at a fixed z as the distance range (Δz) for object is cognizable with CR > 0.5. When the object is closer to the image sensor, the DOF is shorter. Nevertheless, using the tunable lens powers of the LC lens, the DOF can be tuned from 12 to 31 mm accompanied with the shifts of central peaks of the object distance in Fig. 3(a). As a result, the object located between z = 12 mm and z = 51 mm can be imaged by the tunable DOF of the system. Table 1 illustrates the specifications of the LC lens and the corresponding DOF.

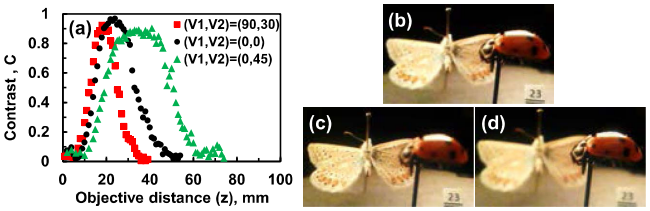

Fig. 3. (a) Contrast ratio as a function of the object distance (z) at different applied voltages. The elemental images captured when the LC lens operates with (b) no lens power at $(V_1, V_2) = (0, 0)$, (c) a negative lens at $(V_1, V_2) = (0, 45\ V_{rms})$, and (d) a positive lens at $(V_1, V_2) = (90\ V_{rms}, 30\ V_{rms})$. A ladybug, a piece of paper printed with "23," and a butterfly used as a 3D scene were located at 14.6 mm, 23 mm, and 42 mm away from the LC lens, respectively.

Table 1. Specification of the LC Lens and the Corresponding DOF

Lens State	Positive	Off	Negative
Applied voltage (V_1, V_2) [V_{rms}]	(90, 30)	(0, 0)	(0, 45)
Object distance [mm]	18	23	38
Depth range [mm]	12–24	15–33	20–51
DOF [mm]	12	18	31

Based on the measurements of the image capture system, we conducted the experiments with a 3D scene. The 3D scene includes three objects placed in front of the LC lens: a ladybug at z = 14.6 mm, a butterfly at z = 42 mm, and a piece of paper printed with the number "23" at z = 23 mm. The CCD size of the endoscope is 1.792 × 1.008 mm. To apply the SAII method, the moving step of the translation stage was set as $(P_H, P_V) = (1.792\ mm, 1.008\ mm)$. Then, two groups of the SAII pickup were conducted under two different voltage conditions of the LC lens. Each set contains 4 (H) × 4 (V) elemental images. We captured elemental images as the LC lens voltage was at $(V_1, V_2) = (0, 0)$, $(0, 45\ V_{rms})$, and $(90\ V_{rms}, 30\ V_{rms})$. The captured images are shown in Figs. 3(b)–3(d). In Fig. 3(b), the LC lens at $(V_1, V_2) = (0, 0)$ has no lens power, and only the piece of paper with "23" at z = 23 mm is clearly imaged while others are blurred due to being outside of the DOF (15–33 mm). In Fig. 3(d), the ladybug at z = 14.6 mm is in focus within the DOF (12–24 mm) as the LC lens is at $(V_1, V_2) = (90\ V_{rms}, 30\ V_{rms})$. At $(V_1, V_2) = (0, 45\ V_{rms})$, the butterfly at 42 mm is clearly imaged within the DOF (20–51 mm), as shown in Fig. 3(c).

Next, we reconstructed the 3D scene computationally. The algorithm we used is based on the ray back-propagation approach [4]. The light from the captured elemental images are inversely traced to reconstruct the 3D scene under the assumption of the pinhole projection model. The reconstructed 3D image is displayed with a series of sliced 2D images of the scene. The computationally reconstructed images are shown in Figs. 4(a) and 4(b). In Fig. 4(a), the image was reconstructed from the elemental image set with the LC lens applied voltage of $(V_1, V_2) = (90\ V_{rms}, 30\ V_{rms})$. The reconstructed image at z = 14.6 mm is in focus with the detailed information of the ladybug. In Fig. 4(b), the reconstructed images at z = 42 mm are in focus for the butterfly with a fine pattern on the wings. The elemental image set for the reconstruction is with the LC

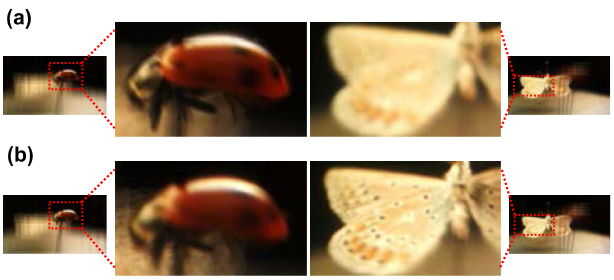

Fig. 4. Experimental results for the 3D SAII endoscopy with the tunable large-aperture LC lens. The computational reconstruction results of two sets of elemental images under two voltage conditions of the LC lens. (a) $(V_1, V_2) = (90\ V_{rms}, 30\ V_{rms})$ and (b) $(0, 45\ V_{rms})$.

lens applied voltage of $(0, 45\ V_{rms})$. These experimental results show the feasibility of our proposed high-resolution extended-DOF 3D SAII endoscopy system.

Finally, we generated a new elemental image array with an extended DOF from the captured elemental images. Assume the source points are Lambertian or semi-Lambertian. With the depth estimation method [17], the depth information corresponding to each pixel of the elemental images can be calculated and stored in another set of 2D images. The 2D images are depth maps. The intensities of the depth map are quantized by the depth information corresponding to the point sources on the object surface. Because of the limitation of the DOF in the pickup process, both focused and defocused regions exist in the captured elemental images. We separated the focused and defocused pixels by comparing the measured DOF with quantized depth information on the depth map. By defining a desired focused depth range (dr) to the depth map, the focused pixels can be extracted from captured elemental images under different applied voltages. A new set of elemental images (EI_{new}) can be generated with an extended DOF. The generation process of EI_{new} can be described as

$$EI_{new}(x,y) = \begin{cases} EI_1(x,y), & DM_1(x,y) \in \mathrm{dr}_1 \\ EI_2(x,y), & DM_2(x,y) \in \mathrm{dr}_2 \\ \cdots & \\ EI_i(x,y), & DM_i(x,y) \in \mathrm{dr}_i \end{cases}, \quad (5)$$

where i indicates the different voltage conditions of the LC lens, (x, y) is the pixel index on a captured $EI_i(x, y)$, and $DM_i(x, y)$ is the corresponding depth map. When the pixels on a captured EI are within the DOF, the pixels are extracted. Figures 5(a) and 5(b) are the elemental images and the corresponding depth maps under the two applied voltage conditions. The generated elemental image is shown in Fig. 5(c). The pixels with focused information were merged together. Thus, the two objects at different image planes can be displayed and visualized simultaneously. The results indicate that we can have an extended-DOF 3D display, and large DOF information can be recorded and visualized. Last but not least, fast imaging speed of the system can be achieved by adopting the overdrive method from display panel and two-mode-switching method [18], or fast-response-time LC lenses, such as FLC lens with response time of 0.171 ms [19], are also the options.

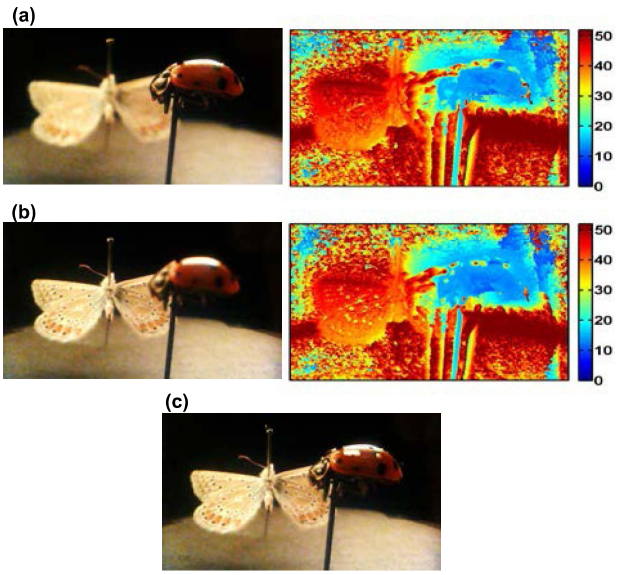

Fig. 5. Three samples of the elemental images and the corresponding depth maps. (a) At $(V_1, V_2) = (90\ V_{rms}, 30\ V_{rms})$, the ladybug is in focus, and the butterfly is out of focus. (b) At $(V_1, V_2) = (0, 45\ V_{rms})$, the ladybug is out of focus, and the butterfly is focused. (c) The merged elemental images with both objects in focus. The color codes indicate the spatial depth information of the 3D scene with a unit of mm.

We have demonstrated an extended-DOF high-spatial-resolution SAII system exploiting an electrically tunable focal-length large-aperture LC Lens for 3D endoscopy. The system can be used for capturing small objects in a short working distance. The focal length is tunable from 18 to 38 mm, and the corresponding DOF can vary from 12 mm (12–24 mm) to 31 mm (20–51 mm). When multiple 3D objects are at different depth positions, we can produce the images in focus of each object by switching the applied voltage to the LC lens. By merging the focused information into a new set of elemental images, the new elemental images contain the focused information with an extended DOF of the 3D scene. This extended-DOF SAII system can operate in a short working distance and makes the 3D integral imaging endoscopy a promising tool for medical applications with high resolution.

Funding. National Science Foundation (NSF) (NSF/IIS-1422179).

Acknowledgment. The authors thank Mr. Hung-Shan Chen for technical assistance. The endoscope is provided by Mr. Paul Chen (NewKen Tech. Co. Ltd.). The specimens are provided by the Biodiversity Collections, UConn.

REFERENCES

1. G. Lippmann, J. Phys. Theory Appl. **7**, 821 (1908).
2. B. Javidi, F. Okano, and J. Y. Son, *Three-Dimensional Imaging, Visualization, and Display* (Springer, 2009).
3. X. Xiao, B. Javidi, M. Martinez-Corral, and A. Stern, Appl. Opt. **52**, 546 (2013).
4. S. Hong, J. Jang, and B. Javidi, Opt. Express **12**, 483 (2004).
5. X. Shen, Y. J. Wang, H. S. Chen, X. Xiao, Y. H. Lin, and B. Javidi, Opt. Lett. **40**, 538 (2015).
6. F. Okano, J. Arai, K. Mitani, and M. Okui, Proc. IEEE **94**, 490 (2006).
7. K. Wakunami, M. Yamaguchi, and B. Javidi, Opt. Lett. **37**, 5103 (2012).
8. R. Martínez-Cuenca, G. Saavedra, M. Martínez-Corral, and B. Javidi, J. Display Technol. **1**, 321 (2005).
9. H. Navarro, G. Saavedra, M. Martínez-Corral, M. Sjöström, and R. Olsson, J. Display Technol. **10**, 182 (2014).
10. J. S. Jang and B. Javidi, Opt. Lett. **29**, 1230 (2004).
11. B. Javidi, S. Yeom, I. Moon, and M. Daneshpanah, Opt. Express **14**, 3806 (2006).
12. A. Hassanfiroozi, Y. P. Huang, B. Javidi, and H. P. D. Shieh, Opt. Express **23**, 971 (2015).
13. J. S. Jang and B. Javidi, Opt. Lett. **27**, 1144 (2002).
14. H. S. Chen and Y. H. Lin, Opt. Express **21**, 18079 (2013).
15. S. Sato, Jpn. J. Appl. Phys. **18**, 1679 (1979).
16. Y. H. Lin and H. S. Chen, Opt. Express **21**, 9428 (2013).
17. M. Daneshpanah and B. Javidi, Opt. Lett. **34**, 1105 (2009).
18. H. C. Lin and Y. H. Lin, Appl. Phys. Lett. **97**, 063505 (2010).
19. H. S. Chen, Y. H. Lin, A. K. Srivastava, V. G. Chigrinov, C. M. Chang, and Y. J. Wang, Opt. Express **22**, 13138 (2014).